

HS-OFDM-based Time-Domain Reflectometry for Power Line Sensing: Characteristics and Limitations

Lucas Giroto de Oliveira, *Student Member, IEEE*, Mateus de L. Filomeno,
and Moisés V. Ribeiro, *Senior Member, IEEE*

Abstract—This study discusses key characteristics and limitations of time-domain reflectometry (TDR) systems based on the Hermitian symmetric orthogonal frequency-division multiplexing (HS-OFDM) scheme for power line sensing. In this sense, a system model with a power line modem injecting signals and capturing raising reflections for sensing a power distribution network is outlined. Next, pulse compression and channel estimation reflectogram processing approaches are carefully described and the effects of system parametrization and multiple access schemes on the HS-OFDM-based TDR system performance are addressed. Finally, numerical results covering a comparison between pulse compression and channel estimation, system limitations based on parametrization considering typical European underground low-voltage and US overhead medium-voltage (MV) scenarios and narrowband (NB) power line communication (PLC) regulatory constraints, and comparison among multiple access techniques in a Brazilian MV overhead scenario are presented for supporting the carried out discussion. Based on the attained results, it is shown that channel estimation outperforms the pulse compression in terms of computational complexity and sidelobe level. Also, it is shown that the NB-PLC frequency range provides fair range resolution and maximum unambiguous range values. Finally, it is seen that the use of the frequency-division multiple access multiple access schemes presents different signal-to-interference-plus-noise ratio (SINR) performance among different power line modems (PLMs) connected to a power distribution grid, while the use of time-division multiple access and code-division multiple access schemes results in fair SINR performance among the PLMs at the cost of obtaining less reflectograms over time due to time multiplexing and spreading processes, respectively.

Index Terms—Time-domain reflectometry, orthogonal frequency-division multiplexing, multiple access, power line communication.

I. INTRODUCTION

Today, electrical energy is a key resource in the entire world. The need to connect power generating units to final consumers has led to a significant expansion of power transmission and distribution infrastructures. Such expansion implies in greater subjectivity of the latter to faults along with both infrastructures. In order to minimize the interruption time as

well as the damages resulting from faults, several protection schemes have been developed.

Conventional protection schemes for power line networks, however, fail in tasks such as detection and location of hard faults, e.g. high impedance faults (HIFs) or distant low impedance faults (LIFs), and soft faults, eg. cable degradation. Among more efficient alternatives are analysis harmonic currents and voltages [1], [2], and the use of traveling waves for detecting and locating impedance discontinuities along the network. The latter, which has long been subject of study for sensing of wired networks in scenarios such as aircraft [3], has been gaining attention for sensing of power lines. In this context, the adaptation of power line modems (PLMs) for network sensing [4] as well as techniques that exploit characteristics of traveling waves propagating back and forward the power line for applications such as topology inference [5] or fault detection and location [6] have been investigated.

Potential techniques for wired network sensing based on traveling waves are impedance spectroscopy, transferometry, and reflectometry [3], [7]. Variations of the latter are time-domain reflectometry (TDR), frequency-domain reflectometry (FDR) [8], and joint time-frequency domain reflectometry (JTFDR) [9], which consist of injecting signals into the analyzed network and capturing the raised reflections, which are respectively processed in time, frequency, or both domains. The use of TDR principles for fault sensing in power lines, subject of study in the past [10], [11], has been recently revisited in the literature [12] due to low computational complexity associated with the post-processing of obtained reflectograms. Such aspect of TDR-based techniques allows on-line obtaining of reflectograms [13], therefore enabling efficient sensing of power line networks at both symbol and mains levels [4].

Effectiveness in terms of digital signal processing and electromagnetic compatibility (EMC) without the inherent drawback of poor spectrum control in classical TDR techniques can be achieved by multicarrier time-domain reflectometry (MCTDR) [14], [15] and its time-domain version [16], which only differ in the domain where reflectogram processing takes place. For enhanced compatibility with existing power line communication (PLC) systems an optimized digital signal processing, an interesting approach is the orthogonal multitone time-domain reflectometry (OMTDR) [13], which is variation of the MCTDR based on orthogonal narrowband frequency-division multiplexing (OFDM).

Although TDR based on OFDM or its baseband version Hermitian symmetric OFDM (HS-OFDM) seems a good can-

Manuscript received MM DD, YYYY; revised MM DD, YYYY. This study was financed in part by the Coordenação de Aperfeiçoamento de Pessoal de Nível Superior - Brasil (CAPES) - Finance Code 001, Copel Distribuição LTD - PD 2866-0420/2015, CNPq, FAPEMIG, INERGE and Smarti9 LTD.

Lucas Giroto de Oliveira and Mateus de L. Filomeno are with the Electrical Engineering Department, Federal University of Juiz de Fora (UFJF), Juiz de Fora, Brazil (e-mail: lgiroto@ieee.org, mateus.lima@engenharia.ufjf.br).

Moisés V. Ribeiro is with the Electrical Engineering Department, Federal University of Juiz de Fora (UFJF), Juiz de Fora, Brazil, and Smarti9 Ltd, Brazil (e-mail: mribeiro@ieee.org).

didate for power line sensing, aspects such as measurement range and number of reflectograms obtained over time become more relevant due to the long distances in power distribution networks and the linear periodically time variant (LPTV) behavior of transfer functions experienced by signals injected by PLMs into the network. To the best of the author's knowledge, the use of channel estimation, performed for communication purposes in PLC systems [17], rather than the usual pulse compression performed for reflectometric sensing in wired networks [13], [18] has also not been addressed in the literature. For an efficient distributed sensing, the effect of multiple access on TDR measurements, already considered for pulse compression TDR in some aspects [13], [19], must also be taken into account for HS-OFDM-based TDR systems relying on channel estimation. Given this context, the present study investigates the influences of the parametrization of an HS-OFDM-based TDR system as well as limitations imposed by multiple access schemes on its performance for power line sensing.

The main contributions of this study are summarized as follows.

- 1) Description of an HS-OFDM-based TDR system sensing a power distribution network. Based on this formulation, we discuss the pulse compression and channel estimation reflectogram processing approaches and analyze the effect of the TDR system parametrization on its performance using peak-to-sidelobe level ratio (PSLR), integrated-sidelobe level ratio (ISLR), range resolution, and maximum unambiguous range as metrics taking into account regulatory constraints and considering typical European underground low voltage (LV) and US overhead medium voltage (MV) scenarios.
- 2) Introduction of time-division multiple access (TDMA), frequency-division multiple access (FDMA), and code-division multiple access (CDMA) multiple access schemes for an HS-OFDM-based TDR system for power line sensing based on the channel estimation procedure and comparative analysis among them in terms of number of obtained reflectograms and signal-to-interference-plus-noise ratio (SINR) considering a Brazilian overhead MV scenario.

Our major findings are as follows:

- 1) Channel estimation outperforms the pulse compression procedure in terms of both computational complexity and sidelobe level, being therefore a more attractive reflectogram processing approach for HS-OFDM-based TDR systems.
- 2) HS-OFDM-based TDR systems operating in the narrow-band (NB)-PLC frequency range are suitable for the sensing of LV and MV power distribution networks sections, offering fair range resolution and maximum unambiguous range values.
- 3) The use of TDMA and CDMA multiple access schemes results in a smaller number of obtained reflectograms over time respectively due to time multiplexing and spreading processes and in a fair SINR level among the multiple PLMs connected to the power distribution

network, being the SINR higher in the CDMA case due to signal-to-noise ratio (SNR) gain provided by this scheme. On the other hand, the use of FDMA results in a higher number of obtained reflectograms over time in comparison with TDMA and CDMA and in higher SINR to PLMs associated with subcarriers in higher frequency bins due to the exponentially decreasing additive noise power spectral density (PSD).

The remainder of this paper is organized as follows. Section II describes the HS-OFDM-based TDR system for sensing of a power distribution network. Section III discusses the pulse compression and channel estimation procedures for reflectogram processing. Next, Section IV addresses the effect of system parametrization on its performance and Section V discusses the use of multiple access schemes for power line sensing with multiple PLMs. A numerical analysis for supporting the carried out discussion is carried out in Section VI. Finally, concluding remarks are placed in Section VII.

Notation

Throughout the paper, $(\cdot)^T$ and $(\cdot)^\dagger$ indicate the transpose and Hermitian transpose operators, respectively; \star is the convolution operator; \odot and \oslash denote the Hadamard product and division, which respectively perform element-wise multiplication and division of two equal-sized matrices; $\mathbb{E}\{\cdot\}$ represents the expectation operator; the M -size discrete Fourier transform (DFT) matrix is denoted by \mathbf{W}_M ; $\mathbf{0}_{a \times b}$ and $\mathbf{1}_{a \times b}$ denote $(a \times b)$ -size matrices respectively composed of zeros and ones.

II. SYSTEM MODEL

Let a baseband TDR system be consisted by a full-duplex PLM connected to a power distribution network, which, at a single given point, injects signals and captures reflections that travel at a phase velocity v_p . Assuming that the injection and subsequent capture of reflections of signals takes place within a coherence time T_c , in which variations in loads or any other element of the network are irrelevant, one can consider the power distribution network as a linear time-invariant (LTI) system. The reflections captured by the PLM from such power distribution network, which are raised by impedance discontinuities along the path traveled by the injected signal, are therefore the output of a reflection channel with impulse response $h_\Gamma(t)$.

Such reflections are quantified via the input reflection coefficient between the PLM of output impedance denoted in the continuous frequency-domain as $Z_{PLM}(f)$ and the power distribution network of input impedance $Z_{in}(f)$, being expressed as [20]

$$\Gamma_{in}(f) = \frac{Z_{in}(f) - Z_{PLM}(f)}{Z_{in}(f) + Z_{PLM}(f)}. \quad (1)$$

From $\Gamma_{in}(f)$, one finally obtains the impulse response of the reflection channel via the inverse Fourier Transform, i.e.,

$$h_\Gamma(t) = \int_{-\infty}^{\infty} \Gamma_{in}(f) e^{j2\pi ft} df. \quad (2)$$

The reflectometric sensing of the power distribution network can therefore be performed via an analysis of the reflections raised by the impedance discontinuities. For this purpose, the considered TDR system is used for obtaining a reflectogram, which is an estimate of the reflection channel impulse response. In this paper, it is assumed that such procedure is performed by an HS-OFDM system that is band-limited to a bandwidth B and has sampling frequency $F_s = 2B$.

The considered HS-OFDM-based TDR system is depicted in Fig. 1, starting with a complex vector $\mathbf{D} = [D_0, D_1, \dots, D_{N-1}]^T$, such that $\mathbf{D} \in \mathbb{C}^{N \times 1}$. This vector is inputted to the function $\mathcal{P}(\cdot)$ that represents, in a condensed form, the digital processing performed at the transmitter side, which is composed by three processing stages. The first one is the Hermitian symmetric mapping $Map(\cdot)$ [21] that transforms \mathbf{D} into the $2N$ -length discrete-frequency domain HS-OFDM symbol $\mathbf{X} = [X_0, X_1, \dots, X_{2N-1}]^T$ such that $\mathbf{X} \in \mathbb{C}^{2N \times 1}$. Next, the inverse discrete Fourier transform (IDFT) transforms \mathbf{X} into the discrete-time domain vector $\mathbf{x} \in \mathbb{R}^{2N \times 1}$, which is real-valued due to the Hermitian symmetry of \mathbf{X} . This is expressed as $\mathbf{x} = \frac{1}{\sqrt{2N}} \mathbf{W}_{2N}^\dagger \mathbf{X}$. Finally, an L_{cp} -length cyclic prefix is appended to \mathbf{x} , resulting in the vector $\mathbf{s} \in \mathbb{R}^{(2N+L_{cp}) \times 1}$. Considering that the reflection channel impulse response has an L_h -length discrete-time domain representation $\mathbf{h}_\Gamma \in \mathbb{R}^{L_h \times 1}$, no intersymbol interference (ISI) is experienced if the constraint $L_{cp} \leq L_h$ is satisfied.

Back to Fig. 1, the discrete-time vector \mathbf{s} undergoes an digital-to-analog conversion, being converted into the continuous-time signal $s(t)$ that is inputted to the reflection channel of impulse response $h_\Gamma(t)$. It is worth highlighting that, in order for the LTI assumption of the reflection channel to hold, the duration of $s(t)$, i.e., the HS-OFDM symbol in the continuous-time domain, $T_{symp} = (2N + L_{cp})T_s$ must satisfy the constraint $T_{symp} \ll T_c$. The first term of the previous expression accounts for the number of samples of the discrete-time vector \mathbf{s} , while $T_s = 1/F_s$ is the sampling period. The resulting signal from the convolution between the transmit signal and the channel is $\tilde{r}(t) = s(t) \star h_\Gamma(t)$. To this signal is added the noise $v(t)$, which is a zero-mean wide-sense stationary (WSS) random process, resulting in the received signal $r(t) = \tilde{r}(t) + v(t)$. Note that, due to the noise presence, $r(t)$ is also a WSS random process.

At the receiver side, the signal $r(t)$ passes through an analog-to-digital converter, originating the discrete-time domain vector $\mathbf{r} \in \mathbb{R}^{(2N+L_{cp}) \times 1}$. Next, \mathbf{r} is inputted to the function $\mathcal{Q}(\cdot)$, which synthesizes the digital processing at the receiver side of the HS-OFDM-based TDR system. The performed processing by this function starts with cyclic prefix removal from \mathbf{r} , which originates the discrete-time domain vector $\mathbf{y} \in \mathbb{R}^{2N \times 1}$.

The operations ranging from the transmitter processing on \mathbf{x} to ultimately obtain \mathbf{y} can be equivalently expressed in the discrete-frequency domain as

$$\mathbf{Y} = \mathbf{X} \odot \mathbf{H}_\Gamma + \mathbf{V}, \quad (3)$$

where $\mathbf{Y} = \frac{1}{\sqrt{2N}} \mathbf{W}_{2N} \mathbf{y}$, $\mathbf{Y} \in \mathbb{C}^{2N \times 1}$, is the discrete-frequency domain representation of \mathbf{y} ;

$\mathbf{H}_\Gamma = \mathbf{W}_{2N} [\mathbf{h}_\Gamma^T \mathbf{0}_{1 \times (2N-L_h)}]^T$, $\mathbf{H}_\Gamma \in \mathbb{C}^{2N \times 1}$, is the $2N$ -length zero-padded version of the L_h -length discrete-frequency equivalent of the reflection channel impulse response $h_\Gamma(t)$; and $\mathbf{V} = \frac{1}{\sqrt{2N}} \mathbf{W}_{2N} \mathbf{v}$, $\mathbf{V} \in \mathbb{R}^{2N \times 1}$ is a vector composed by $2N$ proper Gaussian random variables and $\mathbf{v} \in \mathbb{R}^{2N \times 1}$ is a $2N$ -length discrete-time domain window of the additive noise $v(t)$.

Alternatively, the vector \mathbf{V} can be represented as $\mathbf{V} = [V_0, V_1, \dots, V_{2N-1}]^T$. Each these variables have equal mean $\mathbb{E}\{V_k\} = 0$, $k = 0, \dots, 2N-1$, and different variances $\mathbb{E}\{|V_k|^2\} = \sigma_{V,k}^2$, being uncorrelated in the frequency domain, i.e., $\mathbb{E}\{V_k V_j^*\} = \mathbb{E}\{V_k\} \mathbb{E}\{V_j^*\}$ for $k = 0, \dots, 2N-1$ and $j = 0, \dots, 2N-1$ such that $k \neq j$, $k \neq 2N-j$. Assuming that the two-sided additive noise PSD is flat within each subband, one can represent it as the vector $\mathbf{S}_V = [S_{V,0}, S_{V,1}, \dots, S_{V,2N-1}]^T$, $\mathbf{S}_V \in \mathbb{R}^{2N \times 1}$, where $S_{V,k} = \sigma_{V,k}^2 / (2N \Delta f)$ is the additive noise PSD at the k^{th} subchannel and $\Delta f = F_s / 2N$ is the subcarrier frequency spacing/bandwidth.

The processing performed by $\mathcal{Q}(\cdot)$ is completed with the obtaining of an L_ρ -length reflectogram that is denoted in the discrete-frequency domain as $\mathbf{P} \in \mathbb{C}^{L_\rho \times 1}$, $L_\rho \geq L_h$. This is performed via processing on the discrete-frequency domain vector \mathbf{Y} , in such a way that the influence of the transmit vector \mathbf{X} on it is minimized or eliminated. A proper reflectogram \mathbf{P} must be a good estimate of the reflection channel frequency response \mathbf{H}_Γ and present a high SNR in order for noise effect to be negligible. The processing performed by $\mathcal{Q}(\cdot)$ is finally completed with a IDFT on \mathbf{P} , resulting in the discrete-time domain reflectogram $\rho \in \mathbb{R}^{L_\rho \times 1}$ that is actually used for analyzing the reflections along the network.

After a reflectogram ρ has been obtained, analog counterpart $\rho(t)$ can be yielded in order to reduce the temporal granularity and, as a consequence, the spatial granularity of the reflectogram and the impedance discontinuity location accuracy. This can be performed via sinc interpolation in the time domain by a reconstruction filter [22]. Alternatively, zero-padding can be performed on the discrete-frequency domain vector \mathbf{P} before transforming it to the time domain [23]. Both these alternatives yield valid reflectograms under the condition that the signal has been sampled at sampling rate of at least $F_s = 2B$. A third alternative would be oversampling $r(t)$ at a sampling frequency $F_s = 2\eta B$ [13], which would ultimately yield a reflectogram $\rho \in \mathbb{R}^{\eta L_\rho \times 1}$, $\eta \in \mathbb{R}$, $\eta > 1$, with finer temporal and spatial granularities for higher η values. Although this is a valid alternative, it would yield significantly higher computational complexity, as all processing stages at the receiver would be performed on longer vectors.

The quality of the obtained reflectogram will ultimately depend not only on the SNR level, but also on the processing performed on \mathbf{y} . Given this context, Section III carries out a careful description of two approaches for the obtaining of the reflectogram ρ from the received vector \mathbf{y} performed by $\mathcal{Q}(\cdot)$.

III. REFLECTOGRAM PROCESSING APPROACHES

A conventional procedure for obtaining reflectograms in TDR systems is the pulse compression, which is based on

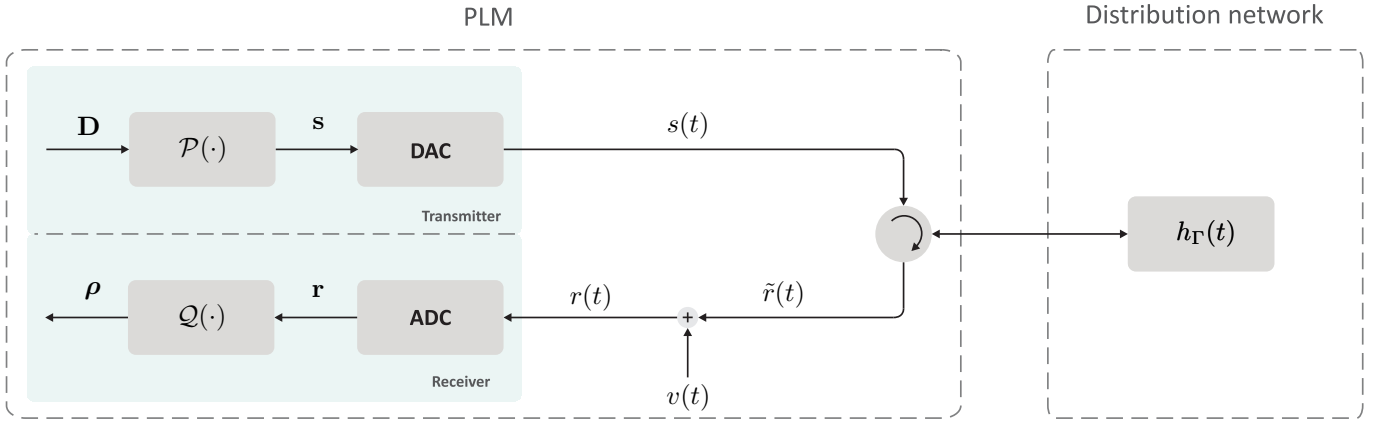


Fig. 1: HS-OFDM-based TDR system over a power distribution network.

the correlation between the transmit and received signals without cyclic prefix, i.e., \mathbf{x} and \mathbf{y} , and has already been addressed in the literature [13], [24]. An alternative processing, usually resorted to in radar systems, consists of obtaining a reflectogram ρ that is an adequate estimate of \mathbf{h}_Γ by removing the effect of the transmit signal on \mathbf{y} via processing in the frequency domain [25]. These two approaches are described in Subsections III-A and III-B, respectively.

A. Pulse compression

The pulse compression consists of correlating the received vector \mathbf{y} with a copy of the transmit vector \mathbf{x} so that the obtained reflectogram ρ is equivalent to the one obtained via the transmission of a narrower pulse, which corresponds to the autocorrelation of \mathbf{x} [8], [13], [26].

Such procedure is performed via a linear convolution between the received \mathbf{y} vector and a matched filter to \mathbf{x} , denoted by $\mathbf{g} \in \mathbb{R}^{2N \times 1}$. This linear convolution can be implemented by means of a circular convolution between $(4N - 1)$ -length zero-padded versions of \mathbf{x} and \mathbf{y} , demanding computational complexity $\mathcal{O}((4N - 1)^2)$ [22], [27]. Alternatively, it can be implemented in the discrete-frequency domain via multiplication of the $(4N - 1)$ -length zero-padded versions of \mathbf{Y} and $\mathbf{G} = \frac{1}{\sqrt{2N}} \mathbf{W}_{2N} \mathbf{g} = [X_0^*, X_1^*, \dots, X_{2N-1}^*]^T$, $\mathbf{G} \in \mathbb{C}^{2N \times 1}$, preceded by a DFT and followed by an IDFT [24], [27]. If fast Fourier transform (FFT) and inverse fast Fourier transform (IFFT) are used, this approach becomes more efficient and faster than the circular convolution in the discrete-time domain [27], imposing the constraint that the zero-padded versions of the aforementioned vectors present length $4N$ and demanding a reduced computational complexity of $\mathcal{O}(2(4N \log_2 4N) + 4N)$.

The $4N$ -length zero-padded versions of \mathbf{Y} and \mathbf{G} are, respectively, $\mathbf{Y}_{ZP} = \frac{1}{\sqrt{4N}} \mathbf{W}_{4N} [\mathbf{y}^T \mathbf{0}_{2N}^T]^T$, $\mathbf{Y}_{ZP} \in \mathbb{C}^{4N}$, and $\mathbf{G}_{ZP} = \frac{1}{\sqrt{4N}} \mathbf{W}_{4N} [\mathbf{g}^T \mathbf{0}_{2N}^T]^T$, $\mathbf{G}_{ZP} \in \mathbb{C}^{4N}$. The resulting reflectogram can therefore be represented in the discrete-frequency domain as

$$\begin{aligned} \mathbf{P}_{PC} &= \mathbf{Y}_{ZP} \odot \mathbf{G}_{ZP} \\ &= \mathbf{R}_{XX,ZP} \odot \mathbf{H}_{\Gamma,ZP} + \mathbf{V}_{ZP} \odot \mathbf{G}_{ZP}, \end{aligned} \quad (4)$$

where \mathbf{P}_{PC} presents length $L_\rho = 4N$, i.e., $\mathbf{P}_{PC} \in \mathbb{C}^{4N \times 1}$; $\mathbf{R}_{XX,ZP} = \mathbf{X}_{ZP} \odot \mathbf{G}_{ZP}$, $\mathbf{R}_{XX,ZP} \in \mathbb{R}^{4N \times 1}$, represents the autocorrelation of \mathbf{x} in the discrete-frequency domain; $\mathbf{X}_{ZP} = \frac{1}{\sqrt{4N}} \mathbf{W}_{4N} [\mathbf{x}^T \mathbf{0}_{2N}^T]^T$, $\mathbf{X}_{ZP} \in \mathbb{C}^{4N}$, is the $4N$ -length zero-padded version of \mathbf{X} ; $\mathbf{H}_{\Gamma,ZP} = \mathbf{W}_{4N} [\mathbf{h}^T \mathbf{0}_{4N-L_h}^T]^T$, $\mathbf{H}_{\Gamma,ZP} \in \mathbb{C}^{4N}$, is the $4N$ -length zero-padded version of \mathbf{h} ; and $\mathbf{V}_{ZP} = \frac{1}{\sqrt{4N}} \mathbf{W}_{4N} [\mathbf{v}^T \mathbf{0}_{2N}^T]^T$, $\mathbf{V}_{ZP} \in \mathbb{C}^{4N}$, is the $4N$ -length zero-padded version of the $2N$ -length noise discrete-time domain window \mathbf{v} in the discrete-frequency domain.

A closer examination of (4) reveals that the obtained reflectogram is biased by the autocorrelation of the transmit signal \mathbf{x} . The resulting reconstructed analog reflectogram $\rho(t)$ obtained by the pulse-compression TDR system will be therefore equivalent to a reflectogram obtained by a conventional TDR system that performs injection of a pulse $s(t) = R_{xx}(t)$ into the network, being $R_{xx}(t)$ the continuous-time domain reconstructed version of the discrete-frequency domain autocorrelation of \mathbf{x} , i.e., $\mathbf{R}_{XX,ZP}$. If $R_{xx}(t)$ presents high PSLR and ISLR values [26], [28], the reflectogram $\rho(t)$ will present significant clutter and the performance of the fault detection and location procedures will therefore be compromised. Such distortion can be minimized by signal processing techniques such as windowing, which reduces the level of sidelobes at the cost of main lobe broadening and consequent resolution loss [13], [29], [30], or designing pulses with desired autocorrelations. The latter approach, however, may limit the use of the HS-OFDM signal to reflectometric sensing, possibly inhibiting its use for communication purposes.

B. Channel estimation

In this approach, the reflectogram ρ is obtained by performing a DFT on \mathbf{y} , followed by a element-wise division of the resulting vector \mathbf{Y} by \mathbf{X} and an IDFT [25]. The resulting operation performed by $\mathcal{Q}(\cdot)$ is therefore equivalent to a channel estimation procedure [17]. The obtained reflectogram can be expressed in the discrete-frequency domain as

$$\begin{aligned} \mathbf{P}_{CE} &= \mathbf{Y} \oslash \mathbf{X} \\ &= \mathbf{H}_\Gamma + \mathbf{V} \oslash \mathbf{X}, \end{aligned} \quad (5)$$

with \mathbf{P}_{CE} presenting length $L_\rho = 2N$, i.e., $\mathbf{P}_{CE} \in \mathbb{C}^{2N \times 1}$.

Finally, the discrete-time domain reflectogram ρ is then simply obtained via a IDFT on \mathbf{P} . If DFT and IDFT are performed by their fast counterparts, i.e., FFT and IFFT, the computational complexity associated with this procedure is $\mathcal{O}(2(2N \log_2(2N)) + 2N)$ due to the two aforementioned stages plus the Hadamard division, being therefore significantly smaller than in the pulse compression case.

Unlike the pulse compression case, the reflectogram from (5) is unbiased. The only factors limiting the reflectogram quality will therefore be SNR level and system bandwidth. The band limiting of the HS-OFDM-based TDR system to a bandwidth B results in a reconstructed analog reflectogram $\rho(t)$ will be equivalent to the one obtained by the injection of $s(t) = B \text{sinc}(Bt)$, $\text{sinc}(t) = \frac{\sin(\pi t)}{\pi t}$, into the network by a conventional TDR system, which is due to the resulting flat, unitary spectral content from the Hadamard division $\mathbf{X} \otimes \mathbf{X}$ that undergoes Hadamard product with \mathbf{H}_Γ in (5). Although clutter level may not be as relevant as in the pulse compression case, it can still be reduced by windowing [31].

IV. SYSTEM PARAMETRIZATION AND LIMITATIONS

For the system described in Section II, which provides a reflectogram via pulse compression and channel equalization approaches described in Section III, a proper parametrization must be performed in order for the resulting reflectogram to be representative of the network, besides achieving desired maximum unambiguous range and range resolution values. This is mainly done by adopting HS-OFDM symbol length $2N$, cyclic prefix length L_{cp} , and occupied frequency bandwidth B values that satisfy the aforementioned constraints, as described in the following subsections.

A. Channel coherence bandwidth

In order for $h(t)$ to be appropriately reconstructed from \mathbf{h} , a further constraint must be satisfied besides the one related to the channel coherence time T_c mentioned in Section II. This constraint is that the frequency resolution, or subcarrier frequency spacing/bandwidth, Δf must be smaller than the reflection channel coherence bandwidth B_{c,H_Γ} , within which the reflection channel frequency response can be considered flat. The reflection channel coherence bandwidth is expressed by [32]

$$B_{c,H_\Gamma} \triangleq \max_{|R_{H_\Gamma}(\Delta f)| \geq \alpha |R_{H_\Gamma}(0)|} \{\Delta f\}, \quad (6)$$

where $0 \leq \alpha \leq 1$ is a threshold and $R_{H_\Gamma}(\Delta f)$ is the frequency correlation function expressed by

$$R_{H_\Gamma}(\Delta f) \triangleq \int_{-\infty}^{\infty} H_\Gamma(f) H_\Gamma^*(f + \Delta f) df. \quad (7)$$

The frequency resolution, i.e., subcarrier frequency spacing/bandwidth, must therefore be set such that $\Delta f \leq B_{c,H_\Gamma}$. As $\Delta f = F_s/(2N)$ and $F_s = 2B$, it holds the constraint

$$N \geq \frac{B}{B_{c,H_\Gamma}}. \quad (8)$$

B. Maximum unambiguous range

The maximum unambiguous range is limited by the length $2N$ of the received vector \mathbf{y} [33]. This is due to the fact that, in both pulse compression and channel equalization approaches, the reflectogram originates from the removal or minimization of the effect of \mathbf{x} on \mathbf{y} . After this is done, the information on the reflection channel impulse response \mathbf{h} will be contained in a $2N$ -length vector. One must therefore have $2N \geq L_h$ in order for no ambiguities to occur in the reflectogram. This holds even for the pulse compression case, where the reflectogram length is only longer due to zero padding.

Additionally, if the cyclic prefix is not long enough, there may be ambiguities in the reflectogram due to ISI [33]. In order to avoid such effect, the cyclic prefix length must satisfy $L_{cp} \geq L_h$. Due to the aforementioned limitations, the maximum unambiguous range in both pulse compression and channel equalization approaches is

$$d_{\max} = \frac{v_p T_s}{2} \min\{2N, L_{cp}\}, \quad (9)$$

i.e., the minimum length between $2N$ and L_{cp} , multiplied by the sampling period T_s and the phase velocity v_p and divided by 2 in order to account for the round trip time of the reflections [26]. Therefore, for a given maximum unambiguous range d_{\max} , one has the constraints

$$N \geq \frac{d_{\max}}{v_p T_s} \quad (10)$$

and

$$L_{cp} \geq \frac{2d_{\max}}{v_p T_s}. \quad (11)$$

C. Range resolution

The range resolution is the capability of resolving close reflections. For an HS-OFDM-based TDR system occupying a frequency bandwidth of B Herz in the baseband, the corresponding range resolution is

$$\delta = \frac{v_p}{4B}, \quad (12)$$

which holds for both pulse compression [26], [34] and channel equalization [25] procedures.

V. MULTIPLE ACCESS SCHEMES

If N_{PLM} PLMs are to operate over a single power distribution network, therefore constituting a distributed HS-OFDM-based TDR system, multiple access schemes must be adopted. The most usual ones are TDMA, FDMA, and CDMA [33], [34].

For the pulse compression processing approach, TDMA, FDMA, and CDMA schemes have already been addressed in the literature [19], [34]. Out of this reason and due to the evident advantages of the channel estimation procedure over the pulse compression pointed out in Section III, the discussion on multiple access schemes for an HS-OFDM-based TDR system presented in the following subsections will be focused on the channel estimation procedure.

A. Time-division multiple access

TDMA is a widely used multiple-input multiple-output (MIMO) scheme in applications such as radar [33] and communications [35]. For N_{PLM} PLMs transmitting and receiving $2N$ -length HS-OFDM symbols, each one of them accessing the same power distribution network in different time slots, there will be no interference among reflectograms of the different PLMs. Furthermore, each of these reflectograms will have the same maximum unambiguous range $d_{\max,TDMA} = d_{\max}$ and range resolution $\delta_{TDMA} = \delta$ exactly as defined in Section IV, being also subject to the channel coherence bandwidth constraint.

In this scheme, there is a number of

$$N_{\rho,TDMA} = \frac{1}{N_{PLM}T_{symp}} \quad (13)$$

obtained measurements per PLM per second. If intended, the PLMs that are not transmitting in the current time slot can also use the received signal from the transmitting PLM for obtaining a transferogram (i.e., channel impulse response between two PLMs), which can be used for data fusion among the PLMs [7]. This would result in a total number of $N_{meas,TDMA} = 1/T_{symp}$ measurements per PLM per second, which is constituted by $N_{\rho,TDMA} = 1/(N_{PLM}T_{symp})$ reflectograms and $N_{t,TDMA} = (N_{PLM} - 1)/(N_{PLM}T_{symp})$ transferograms.

B. Frequency-division multiple access

In the case where different PLMs are to transmit simultaneously, an alternative is the use of the FDMA principle. For better exploiting information on the network, an interleaved FDMA scheme can be used rather than a localized one that allocated adjacent subcarriers to each PLM [13], [36]. In this approach, $2N/N_{PLM}$ interleaved subcarriers are allocated to each PLM in an HS-OFDM-based TDR system with HS-OFDM symbol length $2N$. The resulting reflectogram for each PLM is therefore obtained by discarding the subcarriers allocated to the remaining PLMs and, after obtaining the discrete-frequency domain reflectogram \mathbf{P} , performing a $(2N/N_{PLM})$ -size IDFT on it in order to obtain the discrete-time domain reflectogram ρ . Finally, the obtained $(2N/N_{PLM})$ -length reflectogram ρ undergoes a reconstruction process that will originate $\rho(t)$ as described in Section II.

In the considered Hermitian symmetric orthogonal frequency-division multiple access (HS-OFDMA) scheme, the vector $\mathbf{D} = [D_0, D_1, \dots, D_{N-1}]^T$, $\mathbf{D} \in \mathbb{C}^{N \times 1}$, from Section II is generated via a pre-mapping on a vector $\dot{\mathbf{D}} = [\dot{D}_0, \dot{D}_1, \dots, \dot{D}_N]^T$, $\dot{\mathbf{D}} \in \mathbb{C}^{(N+1) \times 1}$, whose k^{th} sample \dot{D}_k will be ultimately transmitted at the continuous-frequency bin $f_k = k\Delta f$ Hz after all processing and digital-to-analog conversion has been performed at the transmitter side. This pre-mapping is expressed as

$$D_k = \begin{cases} \dot{D}_{k+1}, & k = 0, \dots, N-2 \\ \dot{D}_0 + j\dot{D}_N, & k = N-1 \end{cases}, \quad (14)$$

where $j = \sqrt{-1}$. In order for interference-free operation of the PLMs to take place,

a set $\mathcal{K}_u = \{u, u + N_{PLM}, u + 2N_{PLM}, \dots\}$, $u = 0, \dots, N_{PLM} - 1$, of N/N_{PLM} interleaved samples of $\dot{\mathbf{D}}$ are allocated to the u^{th} PLM. Also, all PLMs place null values at the samples that have not been allocated to it.

Once the discrete-frequency domain reflectogram \mathbf{P} has been obtained at the receiver side, the PLM performs a channel estimation processing on the corresponding samples to the frequency bins allocated to it. Next, \mathbf{P} is transformed into a modified reflectogram according to the mapping

$$\dot{P}_k = \begin{cases} P_k, & k = 0, N \\ 2P_k, & k = 1, \dots, N-1 \end{cases}, \quad (15)$$

in which \dot{P}_k is the k^{th} sample of the modified reflectogram $\dot{\mathbf{P}} = [\dot{P}_0, \dot{P}_1, \dots, \dot{P}_N]^T$, $\dot{\mathbf{P}} \in \mathbb{R}^{(N+1) \times 1}$. Such mapping is performed in order to map a $2N$ -length Hermitian symmetric vector \mathbf{P} into the N -length vector $\dot{\mathbf{P}}$ with no loss of spectral content.

Finally, the u^{th} PLM obtains an L_ρ -length discrete-time domain reflectogram $\rho_u = [\rho_{u,0}, \rho_{u,1}, \dots, \rho_{u,L_\rho}]^T$, $\rho_u \in \mathbb{R}^{L_\rho \times 1}$, $L_\rho = 2N/N_{PLM}$, whose n^{th} sample is expressed as

$$\rho_{u,n} = \frac{1}{\sqrt{L_\rho}} \left[\sum_{k \in \mathcal{K}_u} \Re\{\dot{P}_k\} \cos\left(\frac{\pi kn}{N}\right) - \sum_{k \in \mathcal{K}_u} \Im\{\dot{P}_k\} \sin\left(\frac{\pi kn}{N}\right) \right], \quad (16)$$

which, for the single-PLM case, is exactly the same result obtained by performing an IDFT on \mathbf{P} .

The obtained reflectograms in the proposed HS-OFDMA scheme will have maximum unambiguous range experienced by each PLM equal to $d_{\max,FDMA} = d_{\max}/N_{PLM}$. The range resolution for each PLM in its turn will be $\delta_{FDMA} = v_p/(4B_{FDMA})$, with B_{FDMA} being the effective bandwidth experienced by each PLM. As $2N/N_{PLM}$ subcarriers are allocated to each PLM, the effective subcarrier separation experienced by the latter will be $\Delta f_{FDMA} = N_{PLM}B/N$. Consequently, $B_{FDMA} = N\Delta f_{FDMA}/N_{PLM} = B$, and it holds that the range resolution is exactly as defined in Section IV for the single-user case, i.e., $\delta_{FDMA} = \delta$. Although the range resolution is maintained, the information on the network contained in the subcarriers discarded by the PLM will cause distortion on the obtained reflectograms. The trade-off between number of PLMs connected to the network and reflectogram quality must therefore be observed in order for fault detection and location procedures not to be negatively affected.

As a consequence, one obtains a number of

$$N_{\rho,FDMA} = \frac{1}{T_{symp}} \quad (17)$$

reflectograms per PLM per second. If transferograms are also to be obtained, one would have a total number of $N_{meas,FDMA} = N_{PLM}/T_{symp}$ measurements per PLM per second, encompassing $N_{\rho,FDMA} = 1/T_{symp}$ reflectograms and $N_{t,FDMA} = (N_{PLM} - 1)/T_{symp}$ transferograms.

C. Code-division multiple access

Unlike the TDMA and FDMA schemes, the use of CDMA allows the PLMs to occupy the entire bandwidth over all time slots [19], [33], [34]. The implementation of this scheme consists of adding an encoding process on the discrete-frequency domain vector \mathbf{D} .

In this context, let us consider an N_{PLM} -size Hadamard matrix whose rows are constituted by codewords that are orthogonal among each other. The codeword of the u^{th} row of this matrix, $u = 0, \dots, N_{PLM} - 1$, is represented by the vector $\mathbf{C}_u = [C_{u,0}, C_{u,1}, \dots, C_{u,N_{PLM}-1}]^T$, $\mathbf{C}_u \in \{-1, 1\}^{N_{PLM} \times 1}$, which is in its turn allocated to the u^{th} PLM. Due to the orthogonality among the codewords, the mutual interference among the PLMs is minimized.

The encoding process performed by the u^{th} PLM is then performed via a multiplication between the codeword vector by the transpose counterpart of $\mathbf{D} \in \mathbb{C}^{N \times 1}$, resulting in the spread symbol matrix

$$\mathbf{D}_{C,u} = \mathbf{C}_u \mathbf{D}^T, \quad (18)$$

for which holds $\mathbf{D}_{C,u} \in \mathbb{C}^{N_{PLM} \times N}$. The N_{PLM} rows of this matrix are then sequentially fed to the Hermitian symmetric mapping and further processing, being finally transmitted by the u^{th} PLM. Thus, the resulting transmission time is N_{PLM} times longer than the T_{symp} seconds of the single-PLM case.

After cyclic prefix removal and DFT are performed on the N_{PLM} received symbols at the receiver side, a reception matrix $\mathbf{Y}_C \in \mathbb{C}^{N_{PLM} \times 2N}$ is formed, being its rows associated with the rows of $\mathbf{D}_{C,u}$.

$$\mathbf{Y}_C = \mathbf{X}_C \odot \mathbf{H}_{\Gamma,C} + \mathbf{V}_C + \mathbf{V}_{C,I}, \quad (19)$$

where $\mathbf{X}_C \in \mathbb{C}^{N_{PLM} \times 2N}$ is a transmission matrix whose rows result from the Hermitian symmetric mapping on the respective rows of $\mathbf{D}_{C,u}$; $\mathbf{H}_{\Gamma,C} \in \mathbb{C}^{N_{PLM} \times 2N}$ is an equivalent reflection channel matrix, expressed as $\mathbf{H}_{\Gamma,C} = \mathbf{1}_{N_{PLM} \times 1} \mathbf{H}_{\Gamma}^T$; $\mathbf{V} \in \mathbb{C}^{N_{PLM} \times 2N}$ is a noise matrix whose rows are $2N$ -length discrete-frequency domain windows of the additive noise $v(t)$; and \mathbf{V}_I is the interference noise matrix, which accounts for the mutual interference among the PLMs. The u^{th} PLM then performs a decoding process on \mathbf{Y}_C , which generates the vector $\mathbf{Y} \in \mathbb{C}^{2N \times 1}$ and is expressed as

$$\mathbf{Y} = \frac{(\mathbf{C}_u^T \mathbf{Y}_C)^T}{|\mathbf{C}_u|}, \quad (20)$$

where $|\mathbf{C}_u| = \mathbf{C}_u^T \mathbf{C}_u$ is the cardinality of the codeword vector \mathbf{C}_u . The discrete-frequency domain vector \mathbf{Y} can be alternatively expressed as

$$\mathbf{Y} = \mathbf{X} \odot \mathbf{H}_{\Gamma} + \hat{\mathbf{V}} + \hat{\mathbf{V}}_I, \quad (21)$$

in which $\hat{\mathbf{V}} = (\mathbf{C}_u^T \mathbf{V}_C)^T / |\mathbf{C}_u|$ is the resulting additive noise from the decoding process, whose PSD is expressed as $\mathbf{S}_{\hat{\mathbf{V}}} = [S_{\hat{\mathbf{V}},0}, S_{\hat{\mathbf{V}},1}, \dots, S_{\hat{\mathbf{V}},2N-1}]^T$, $\mathbf{S}_{\hat{\mathbf{V}}} \in \mathbb{R}^{2N \times 1}$, with $S_{\hat{\mathbf{V}},k} = (\sigma_{\hat{\mathbf{V}},k}^2 / \sqrt{N_{PLM}}) / (2N \Delta f)$ representing the resulting additive noise PSD at the k^{th} subchannel; and $\hat{\mathbf{V}}_I = (\mathbf{C}_u^T \mathbf{V}_{C,I})^T / |\mathbf{C}_u|$ is the resulting interference noise. The fact that the resulting additive noise has variance and therefore PSD $\sqrt{N_{PLM}}$ times smaller than the ones of the

original additive noise \mathbf{V} is due to the averaging process that happens at the decoding stage of the CDMA scheme in (20) and ultimately results in an SNR gain [19].

After this stage, a channel estimation procedure is performed on \mathbf{Y} as described in Subsection III-B for the single-PLM case. The resulting discrete-frequency domain reflectogram \mathbf{P} finally undergoes an IDFT, originating the discrete-time domain reflectogram ρ . Although the effect of the transmit symbol on the reflectogram is properly removed, the use of CDMA introduces mutual interference among the PLMs, whose reflectograms consist of the reflections raised by the injected signal by the own PLM plus a term that accounts for the decoded symbols transmitted by the remaining PLMs as well as additive noise. Despite being significantly attenuated by the decoding process, this interference term might distort the obtained reflectogram [33].

In spite of the undesired interference, the obtained reflectograms in the CDMA scheme yield the same maximum unambiguous range $d_{\max,CDMA} = d_{\max}$ and range resolution $\delta_{CDMA} = \delta$ as in the single-user case from Section IV, whose channel coherence bandwidth constraint still holds. Due to the extended transmission time, a number

$$N_{\rho,CDMA} = \frac{1}{N_{PLM} T_{symp}} \quad (22)$$

of reflectograms are obtained per PLM per second. In the case where transferograms are also obtained, the total number of measurements per PLM per second would be $N_{meas,CDMA} = 1/T_{symp}$ measurements, which encompasses $N_{\rho,CDMA} = 1/(N_{PLM} T_{symp})$ reflectograms and $N_{t,CDMA} = (N_{PLM} - 1)/(N_{PLM} T_{symp})$ transferograms.

VI. NUMERICAL ANALYSIS

In this section, the carried out discussion on reflectogram processing approaches and multiple access schemes throughout the paper is validated via numerical results. Given this context, Subsection VI-A compares the pulse compression and channel estimation procedures, while Subsection VI-B addresses system limitations due to regulatory constraints. Finally, the discussed multiple access schemes are analyzed in Subsection VI-C.

A. Pulse compression and channel estimation comparison

In order to corroborate with the claim that the channel estimation procedure outperforms the classical pulse compression for TDR, Fig. 2 presents a comparison of both approaches in terms of computational complexity. Based on the expressions provided in Subsections III-A and III-B, a far higher computational complexity is demanded by the pulse compression approach as it is performed on a longer vector.

Furthermore, the claim that the quality of obtained reflectograms is higher in the channel estimation procedure is endorsed by the results from Figs. 3 and 4. In these figures, PSLR and ISLR values are respectively shown for the equivalent transmit pulse $s(t) = R_{xx}(t)$ obtained via pulse compression and the equivalent transmit pulse $s(t) = B \text{sinc}(Bt)$ for the channel estimation procedure. In this figure, typical modulations schemes for PLC systems, namely binary phase-shift

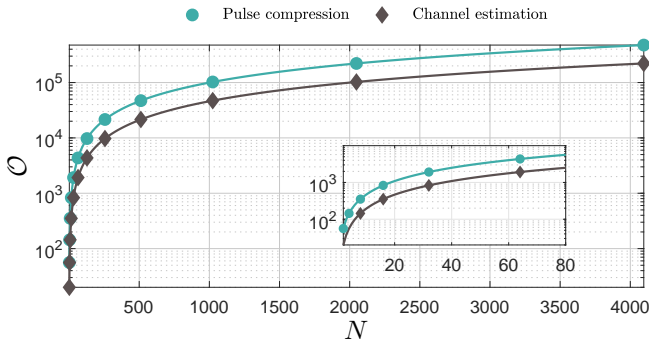


Fig. 2: Computational complexity (disregarding signal reconstruction) as a function of N for the two reflectogram processing approaches.

keying (BPSK), quadrature phase-shift keying (QPSK), and eight phase-shift keying (8PSK) [37], are considered for the pulse compression approach, being the results for the channel estimation approach independent of the adopted scheme.

The attained results show that the PSLR decreases with the modulation order for the pulse compression approach. As N increases, the difference among the PSLR values yielded by either pulse compression or channel estimation becomes negligible. Finally, it is observed that PSLR levels decrease inversely along with N .

Regarding ISLR, the attained values also decrease with the modulation order for the pulse compression procedure, being the difference between QPSK and 8PSK more subtle. The best ISLR values are attained by the channel estimation procedures, which significantly outperforms the pulse compression procedure by about 6.4 dB if QPSK and 8PSK are assumed for the latter, and by 8.9 dB if pulse compression is performed on a signal belonging to a BPSK modulation. Unlike the PSLR case, there is a slight increase of ISLR values along with N . This is explained by the fact that, given a fixed B , the side lobe level is increased, while the main lobe duration of $1/(2B)$ seconds and therefore the main lobe level are maintained for longer HS-OFDM symbols.

B. System limitations

Although an adequate parametrization of the HS-OFDM-based TDR system can yield valid reflectograms, regulatory constraints limit the PSLR and ISLR values, as well as achievable range resolution and maximum unambiguous range. The latter two parameters are also influenced by characteristics of the cable where the injected signal propagates, which define the phase velocity v_p . An awareness of such limitations is therefore paramount for performing adequate sensing of the power distribution network.

In this context, two scenarios are addressed, namely an European underground low-voltage power distribution network and an US overhead medium-voltage power distribution network in a rural area. For the low-voltage scenario, it is considered a power supply cable NAYY150SE with resistance R' , inductance L' , conductance G' , and capacitance C' per unit length calculated as in [38], whereas for the medium-voltage cable, the power supply cable with distributed param-

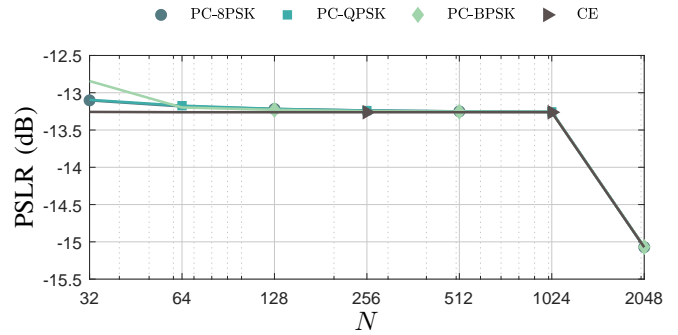


Fig. 3: PSLR as a function of the number of subcarriers N for the pulse compression procedure with BPSK, QPSK, and 8PSK modulations, and for the channel estimation procedure.

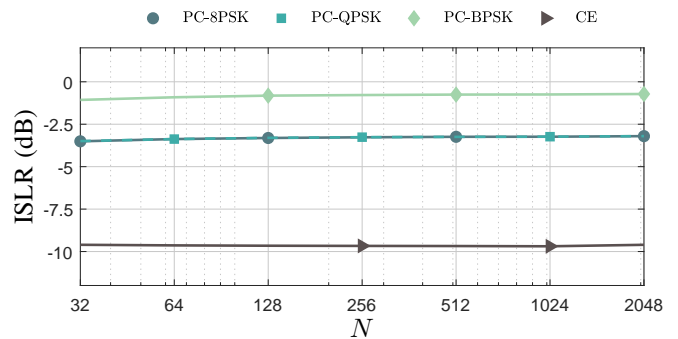


Fig. 4: ISLR as a function of the number of subcarriers N for the pulse compression procedure with BPSK, QPSK, and 8PSK modulations, and for the channel estimation procedure.

eters listed in [37] is adopted. Based on these parameters, the phase velocity is calculated by $v_p = 1/\sqrt{L'C'}$ [20], resulting in $v_p = 1.50 \times 10^8$ for the considered LV cable, and $v_p = 2.56 \times 10^8$ for the considered MV cable.

Fig. 5 shows the range resolution δ as a function of the occupied frequency bandwidth B for the considered LV and MV scenarios. The achieved δ values range from tens of thousands of kilometers for low B values to a few meters for higher B values, with a ratio of 1.71 between the resolution in the MV and LV and scenarios due to their different phase velocity. The presented results indicate that B values in the NB-PLC frequency range, i.e., $B < 500$ kHz, result in fair range resolution values, i.e., $\delta \geq 75$ m, and therefore a fair capability of resolving close impedance discontinuities for typical distances covered by PLC signaling in LV and MV power distribution networks, which are about 1 km in MV scenarios and shorter in LV scenarios [4], [39].

For typical PLC systems, one observes $2N > L_{cp}$. As a consequence, only L_{cp} limits d_{\max} according to the relation in (9). Based on this assumption and considering typical sampling frequency values for NB-PLC, namely $F_s = 0.4$ MHz and $F_s = 1.2$ MHz, Fig. 6 shows the maximum unambiguous range d_{\max} as a function of the cyclic prefix length in the considered LV and MV scenarios. In this figure, one observes a minimum d_{\max} value of about 1 km for $L_{cp} \geq 16$, which is experienced with $F_s = 1.2$ MHz in the LV scenario. For

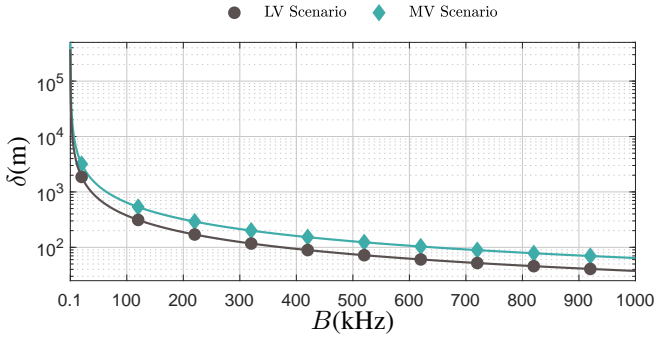


Fig. 5: Range resolution δ in meters as a function of the occupied frequency bandwidth B in the considered LV and MV scenarios.

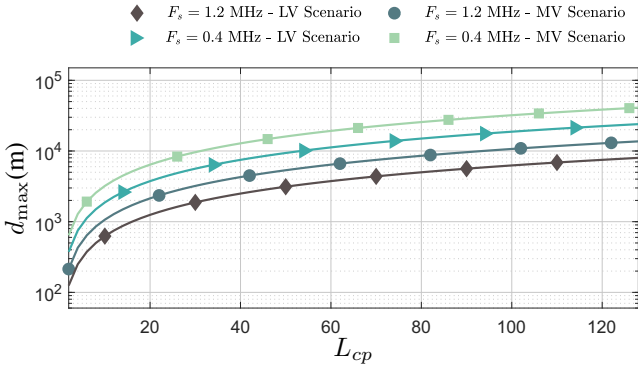


Fig. 6: Maximum unambiguous range d_{\max} as a function of cyclic prefix length L_{cp} for a sampling frequency $F_s = 1.2$ MHz.

$L_{cp} \geq 64$, it holds $d_{\max} \geq 4$ km for both considered sampling frequencies in both LV and MV scenarios. As the typical spacing between PLMs in a power distribution network is considerably shorter than that, these results show that typical cyclic prefix lengths for NB-PLC systems, i.e., $L_{cp} = 32$ and $L_{cp} = 50$, are enough for providing fair maximum unambiguous range values.

Focusing on regulatory constraints, the considered regulations in this paper are Federal Communications Commission (FCC), Association of Radio Industries and Businesses (ARIB), and European Committee for Electrotechnical Standardization (*Comité Européen de Normalisation Électrotechnique* in French) (CENELEC), which are addressed in the IEEE 1901.2 Standard [37] for NB-PLC. The frequency range, occupied frequency bandwidth B , sampling frequency F_s , FFT/IFFT size, range and number of active subcarriers N_{active} , and cyclic prefix length L_{cp} associated with these regulations are listed in Table I. In this table, the a number of ative subcarriers N_{active} is adopted for both FCC and ARIB regulations for covering the whole frequency band covered by these regulations described in [37]. Also, the whole CENELEC band is considered, i.e., from the lowest frequency of the CENELEC A band to the highest frequency of the CENELEC D band, being the adopted number of active subcarriers equal to the necessary for covering this whole frequency bandwidth. For HS-OFDM-based TDR systems parametrized according

to these three regulations, Table II lists the achieved PSLR and ISLR values, as well as range resolution and maximum unambiguous range for the considered LV and MV scenarios. Based on the data of this table, one can conclude that FCC and ARIB regulations allow a more appropriate sensing of shorter power distribution network sections than CENELEC, providing finer range resolution and shorter maximum unambiguous range. Also, adopting the long L_{cp} of both FCC and ARIB regulations results in a significant increase of d_{\max} at the cost of obtaining less reflectograms over time due to the transmission of more cyclic prefix samples.

C. Channel estimation with multiple access

For a comparison among the three multiple access schemes described in Section V that allow the simultaneous obtaining of reflectograms by multiple PLMs connected to the same power distribution network, an HS-OFDM-based TDR system parametrized according to the FCC regulation is considered in this subsection. Additionally, BPSK modulation scheme was adopted.

In this context, simulations were carried out based on an multiconductor transmission line (MTL)-based model [20], [40] of a real MV power distribution network section in the city of Curitiba, Brazil, depicted in Fig. 7. This section is consisted by a feeder, which is an high voltage (HV)/MV transformer, followed by 2.73 km of line and a delta load. The input impedance of the HV/MV transformer at the MV side, as well as the input impedance of the network after the delta load are assumed to be much higher than the characteristic impedance of the line, thus behaving as an open circuit. Two PLMs are connected to this network right after the feeder, being one connected between phases A and B and the other between phases C and B. After an 1 km line section, other PLMs are connected to the network between the same pairs of phases. Thus, there is a line section with length of 1.73 km between the latter PLMs and the delta load. Regarding the additive noise, the adopted model is the one reported in [41], [42], which presents one-sided PSD in the continuous-frequency domain equal to $S_V(f) = -93 + 52.98e^{-0.0032f/10^3}$ dBm/Hz.

The number of reflectograms obtained over time N_ρ , which varies due to the different procedures adopted by the multiple access schemes for providing orthogonality among the signals

TABLE I: Adopted HS-OFDM system parameters according to NB-PLC regulations.

Regulation		FCC	ARIB	CENELEC
Frequency range (kHz)		10 – 490	10 – 450	3 – 148.5
B (kHz)		480	440	145.5
F_s (MHz)		1.2	1.2	0.4
FFT/IFFT size		256	256	256
Active subcarriers		3 – 104	3 – 96	2 – 95
N_{active}		102	94	94
L_{cp}	Standard	30	30	30
	Long	52	52	-

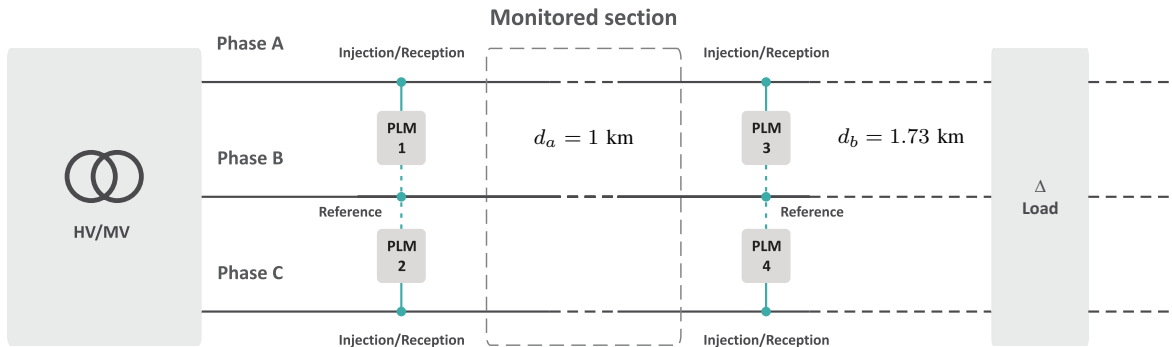


Fig. 7: Considered MV distribution network section.

of the multiple PLMs, is shown in Fig. 8 as a function of the number of PLMs N_{PLM} for both standard and short cyclic prefix lengths. In this figure, one observes decreasing N_ρ values along with N_{PLM} for both TDMA and CDMA schemes, while the FDMA scheme presents constant N_ρ regardless of the number N_{PLM} of PLMs. This happens due to the long time interval during which a PLM does not transmit signals in the TDMA scheme. The lower N_ρ values in the CDMA scheme are on the other hand due to the spreading of HS-OFDM symbols, which results in longer effective transmission time for HS-OFDM symbols in this scheme. It is worth highlighting that, for a given N_{PLM} , the number of obtained reflectograms N_ρ is the same for both TDMA and CDMA schemes.

As previously mentioned, the use of FDMA results in a fixed N_ρ . This is shown in Fig. 8 based on the assumption that $N \geq N_\rho$, i.e., the number of subcarriers is not less than the number of PLMs. Nevertheless, the obtained reflectograms by each PLM will be distorted if the number of subcarriers N/N_{PLM} ($128/N_{PLM}$ in the FCC case) assigned to each of them does not satisfy both the reflection channel coherence bandwidth constraint from (8) and the maximum unambiguous range constraint from (10), being the latter only relevant if $2N/N_{PLM} < L_{cp}$ due to the relationship from (9).

A further analysis is a comparison of the TDMA, FDMA, and CDMA multiple access schemes considering an one-sided transmit signal PSD of -36.81 dBm/Hz. Consequently, the total transmission power allocated to all active subcarriers

of each PLMs considering the FDMA scheme is therefore 13.98 dBm, while a total of 20 dBm are allocated to each PLM in the TDMA and CDMA schemes. In order to assess the performance of the aforementioned schemes, the SINR of the discrete-frequency domain received vector \mathbf{Y} was adopted as a metric. For TDMA and FDMA schemes, the SINR for each PLMs is equal to the ratio between the total received signal power and the total additive noise power, being equivalent the overall SNR considering the allocated subcarriers to them. The CDMA case, on the other hand, has also an interference noise term resulting from the decoding process from (20) and pointed out in (21). As a consequence, the SINR at the four PLMs is equal to the ratio between their associated total received signal power and the total additive noise plus interference noise power.

The attained SINR values are listed in Table III. The lower SINR experienced by the PLMs in the TDMA scheme is due to the fact that the whole additive noise spectral content impairs the captured signal from the reflection channel. Meanwhile, the subcarrier hopping in the FDMA scheme results in higher SINR. This is due to the fact that greater part of the additive noise power is concentrated in lower frequencies as its PSD decreases exponentially. As a consequence, the subcarrier hopping makes the PLMs experience less effective noise power and therefore increases the SINR in comparison to the TDMA scheme. The increasing SINR along with the PLM

TABLE II: Resulting range resolution in LV and MV scenarios, PSLR, and ISLR for NB-PLC regulations.

Regulation		FCC	ARIB	CENELEC	
δ (m)	LV	78.07	85.17	257.56	
	MV	133.59	145.73	440.70	
d_{\max} (km)	Std. L_{cp}	LV	1.87	1.87	5.62
		MV	3.21	3.21	9.62
	Long L_{cp}	LV	3.25	3.25	-
		MV	5.56	5.56	-
Sidelobe level	PSLR (dB)	-13.26	-13.26	-13.26	
	ISLR (dB)	-9.66	-9.66	-9.66	

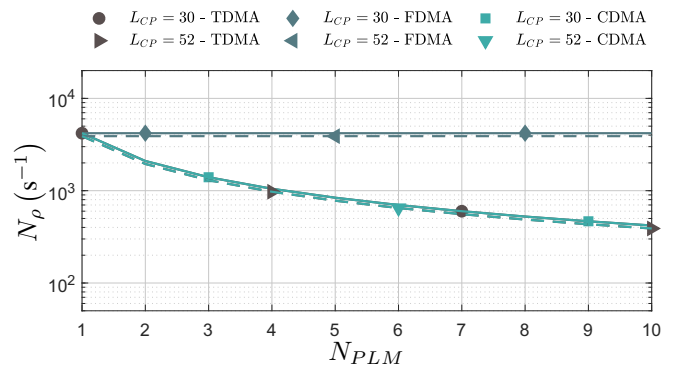


Fig. 8: Number of obtained reflectograms N_ρ as a function of the number of PLMs N_{PLM} for the considered multiple access schemes and cyclic prefix lengths.

TABLE III: SINR at the four PLMs for the considered multiple access schemes.

PLM index u	1	2	3	4
TDMA	28.1595dB	28.1581dB	28.1595dB	28.1581dB
FDMA	29.3370dB	29.8451dB	31.9130dB	32.6272dB
CDMA	31.1698dB	31.1684dB	31.1698dB	31.1684dB

index u is due to the fact that subcarriers belonging to the set \mathcal{K}_u allocated to the u^{th} PLM are associated to higher frequency bins $f_k = k\Delta f$ as u increases, which is described in Subsection V-B and results in lower effective additive noise power for higher u . Finally, the higher average SINR among the PLMs in the CDMA scheme is due to the SNR gain due to noise averaging in the decoding process, as described in Subsection V-C.

VII. CONCLUSION

This study has discussed the main aspects of an HS-OFDM-based TDR system for power line sensing. In summary, a system model covering the injection of HS-OFDM signals into the power distribution grid and subsequent reception of raised reflections has been outlined and pulse compression and channel estimation approaches for obtaining reflectograms have been discussed. Also, limitations of the TDR system based on its parametrization and multiple access schemes have been addressed.

The carried out discussion has been supported by numerical results, which has shown the superiority of the channel estimation procedure over the pulse compression. Furthermore, the influence of the TDR system parametrization on sidelobe level, range resolution, and maximum unambiguous range. The attained results show that the NB-PLC frequency range is suitable for the sensing of LV and MV power distribution networks, with the appropriate frequency bandwidth for monitoring a power distribution network section being inversely proportional to its length. For the latter analysis, typical European underground LV and US overhead MV scenarios have been considered and compliance to FCC, ARIB, and CENELEC NB-PLC regulations has also been addressed.

Finally, a comparison among multiple access schemes has been performed considering a Brazilian overhead MV scenario. It has been shown that TDMA offers a fair SINR level for all PLMs sensing a power distribution network, while the use of FDMA results in higher SINR to PLMs associated with subcarriers in higher frequency bins due to the exponentially decreasing additive noise PSD. The attained SINR levels by the PLMs in CDMA scheme is higher than in the other schemes and fair among the PLMs, which is due to the averaging process that lowers the additive noise PSD in the decoding stage. Additionally, a higher number of reflectograms, which may be distorted if the reflection channel coherence bandwidth constraint is not observed, is obtained over time in the FDMA scheme. TDMA and CDMA schemes, however, obtain less but non-distorted reflectograms due to time multiplexing and spreading processes.

REFERENCES

- [1] M. Sedighizadeh, A. Rezaadeh, and N. I. Elkalashy, "Approaches in high impedance fault detection - a chronological review," *Advances in Electrical and Computer Engineering*, vol. 10, no. 3, pp. 114–128, Aug 2010.
- [2] A. Ghaderi, H. L. Ginn, and H. A. Mohammadpour, "High impedance fault detection: A review," *Electric Power Systems Research*, vol. 143, pp. 376 – 388, Feb. 2017.
- [3] F. Auzanneau, "Wire troubleshooting and diagnosis: Review and perspectives," *Progress In Electromagnetics Research B*, vol. 49, pp. 253–279, 2013.
- [4] F. Passerini and A. M. Tonello, "Smart grid monitoring using power line modems: Anomaly detection and localization," *Cornell University Library*, pp. 1–8, July 2018. [Online]. Available: <https://arxiv.org/abs/1807.05347>
- [5] M. O. Ahmed and L. Lampe, "Power line communications for low-voltage power grid tomography," *IEEE Transactions on Communications*, vol. 61, no. 12, pp. 5163–5175, Dec. 2013.
- [6] A. N. Milioudis, G. T. Andreou, and D. P. Labridis, "Detection and location of high impedance faults in multiconductor overhead distribution lines using power line communication devices," *IEEE Transactions on Smart Grid*, vol. 6, no. 2, pp. 894–902, March 2015.
- [7] F. Auzanneau, "Transferometry: A new tool for complex wired networks diagnosis," *Progress In Electromagnetics Research B*, vol. 70, pp. 87–100, 2016.
- [8] C. Furse, Y. Chung, C. Lo, and P. Pendayala, "A critical comparison of reflectometry methods for location of wiring faults," *Smart Structures and Systems*, vol. 2, no. 1, pp. 25–46, Jan. 2006.
- [9] J. Wang, P. E. C. Stone, Y. . Shin, and R. A. Dougal, "Application of joint time-frequency domain reflectometry for electric power cable diagnostics," *IET Signal Processing*, vol. 4, no. 4, pp. 395–405, Aug. 2010.
- [10] V. Taylor and M. Faulkner, "Line monitoring and fault location using spread spectrum on power line carrier," *IEE Proceedings - Generation, Transmission and Distribution*, vol. 143, no. 5, pp. 427–434, Sept. 1996.
- [11] Z. Q. Bo, G. Weller, and M. A. Redfern, "Accurate fault location technique for distribution system using fault-generated high-frequency transient voltage signals," *IEE Proceedings - Generation, Transmission and Distribution*, vol. 146, no. 1, pp. 73–79, Jan 1999.
- [12] F. de Paulis, C. Olivieri, A. Orlandi, and G. Giannuzzi, "Detectability of degraded joint discontinuities in HV power lines through TDR-like remote monitoring," *IEEE Transactions on Instrumentation and Measurement*, vol. 65, no. 12, pp. 2725–2733, Dec 2016.
- [13] W. B. Hassen, F. Auzanneau, L. Incarbone, F. Pères, and A. P. Tchangani, "Distributed sensor fusion for wire fault location using sensor clustering strategy," *International Journal of Distributed Sensor Networks*, vol. 11, no. 4, pp. 1–17, April 2015.
- [14] S. Naik, C. M. Furse, and B. Farhang-Boroujeny, "Multicarrier reflectometry," *IEEE Sensors Journal*, vol. 6, no. 3, pp. 812–818, June 2006.
- [15] P. Amini, C. Furse, and B. Farhang-Boroujeny, "Filterbank multicarrier reflectometry for cognitive live wire testing," *IEEE Sensors Journal*, vol. 9, no. 12, pp. 1831–1837, Dec. 2009.
- [16] A. Lelong and M. O. Carrion, "On line wire diagnosis using multicarrier time domain reflectometry for fault location," in *Proc. IEEE SENSORS*, Oct. 2009, pp. 751–754.
- [17] T. R. Oliveira, C. A. G. Marques, W. A. Finamore, S. L. Netto, and M. V. Ribeiro, "A methodology for estimating frequency responses of electric power grids," *Journal of Control, Automation and Electrical Systems*, vol. 25, no. 6, pp. 720–731, Dec. 2014.
- [18] S. J. Chang, C. K. Lee, C. Lee, Y. J. Han, M. K. Jung, J. B. Park, and Y. Shin, "Condition monitoring of instrumentation cable splices using kalman filtering," *IEEE Transactions on Instrumentation and Measurement*, vol. 64, no. 12, pp. 3490–3499, Dec. 2015.
- [19] A. Lelong, L. Sommervogel, N. Ravot, and M. O. Carrion, "Distributed reflectometry method for wire fault location using selective average," *IEEE Sensors Journal*, vol. 10, no. 2, pp. 300–310, Feb. 2010.
- [20] C. R. Paul, *Analysis of Multiconductor Transmission Lines, 2nd Edition*. John Wiley & Sons Inc., 2007.
- [21] L. G. de Oliveira, G. R. Colen, A. J. H. Vinck, and M. V. Ribeiro, "Resource allocation in HS-OFDM-based PLC systems: A tutorial," *Journal of Communication and Information Systems*, vol. 33, no. 1, Oct. 2018.
- [22] S. K. Mitra, *Digital Signal Processing: A Computer-Based Approach, 4th Edition*. McGraw-Hill, 2010.

- [23] F. Passerini and A. M. Tonello, "Power line fault detection and localization using high frequency impedance measurement," in *Proc. IEEE International Symposium on Power Line Communications and its Applications (ISPLC)*, April 2017, pp. 1–5.
- [24] W. B. Hassen, M. Kafal, and E. Cabanillas, "Time reversal applied to multi-carrier reflectometry for on-line diagnosis in complex wiring systems," in *Proc. IEEE AUTOTESTCON*, Sept. 2018, pp. 1–7.
- [25] C. Sturm, E. Pancera, T. Zwick, and W. Wiesbeck, "A novel approach to OFDM radar processing," in *Proc. IEEE Radar Conference*, May 2009, pp. 1–4.
- [26] L. G. de Oliveira, M. de L. Filomeno, L. F. Colla, H. V. Poor, and M. V. Ribeiro, "On the suitability of PLC pulses for power line fault sensing via time-domain reflectometry," *Cornell University Library*, pp. 1–13, Jan. 2019. [Online]. Available: <https://arxiv.org/abs/1901.07923>
- [27] J. P. Fitch, *Synthetic Aperture Radar*, C. Burrus, Ed. Springer-Verlag, 1988.
- [28] G. Lellouch, A. K. Mishra, and M. Inggs, "Design of OFDM radar pulses using genetic algorithm based techniques," *IEEE Transactions on Aerospace and Electronic Systems*, vol. 52, no. 4, pp. 1953–1966, Aug. 2016.
- [29] M. A. Richards, J. A. Scheer, and W. A. Holm, *Principles of Modern Radar - Basic Principles*. Scitech Publishing Inc., 2010, vol. 1.
- [30] C. L. Temes, "Sidelobe suppression in a range-channel pulse-compression radar," *IRE Transactions on Military Electronics*, vol. MIL-6, no. 2, pp. 162–169, April 1962.
- [31] Y. L. Sit, "MIMO OFDM radar-communication system with mutual interference cancellation," Ph.D. dissertation, Karlsruhe Institute of Technology, Germany, 2017.
- [32] G. R. Colen, L. G. de Oliveira, A. J. H. Vinck, and M. V. Ribeiro, "A spectral compressive resource allocation technique for PLC systems," *IEEE Transactions on Communications*, vol. 65, no. 2, pp. 816–826, Feb. 2017.
- [33] B. Nuss, J. Mayer, and T. Zwick, "Limitations of MIMO and multi-user access for OFDM radar in automotive applications," in *Proc. IEEE MTT-S International Conference on Microwaves for Intelligent Mobility*, April 2018, pp. 1–4.
- [34] W. B. Hassen, "Étude de stratégies de diagnostic embarqué des réseaux filaires complexes," Ph.D. dissertation, University of Toulouse, France, 2014, in French.
- [35] M. de L. Filomeno, G. R. Colen, L. G. de Oliveira, and M. V. Ribeiro, "Two-stage single-relay channel model for in-home broadband PLC systems," *IEEE Systems Journal (Early Access)*, pp. 1–11, July 2018.
- [36] C. Sturm, Y. L. Sit, M. Braun, and T. Zwick, "Spectrally interleaved multi-carrier signals for radar network applications and multi-input multi-output radar," *IET Radar, Sonar Navigation*, vol. 7, no. 3, pp. 261–269, March 2013.
- [37] "IEEE standard for low-frequency (less than 500 kHz) narrowband power line communications for smart grid applications," *IEEE Std 1901.2-2013*, pp. 1–269, Dec. 2013.
- [38] L. Lampe and A. J. H. Vinck, "On cooperative coding for narrow band PLC networks," *AEU - International Journal of Electronics and Communications*, vol. 65, no. 8, pp. 681–687, Aug. 2011.
- [39] L. Lampe, A. M. Tonello, and T. G. Swart, *Power Line Communications: Principles, Standards and Applications from Multimedia to Smart Grid, 2nd Edition*. John Wiley & Sons Inc., 2016.
- [40] L. Franek and P. Fiedler, "A multiconductor model of power line communication in medium-voltage lines," *Energies*, vol. 10, no. 6, pp. 1–16, 2017.
- [41] Z. Tao, Y. Xiaoxian, Z. Baohui, N. H. Xu, F. Xiaoqun, and L. Changxin, "Statistical analysis and modeling of noise on 10-kv medium-voltage power lines," *IEEE Transactions on Power Delivery*, vol. 22, no. 3, pp. 1433–1439, July 2007.
- [42] M. Giroto and A. M. Tonello, "EMC regulations and spectral constraints for multicarrier modulation in PLC," *IEEE Access*, vol. 5, pp. 4954–4966, Mar. 2017.